doi: 10.82124/CEAS-GNC-2026-102 CEAS-GNC-2026-102

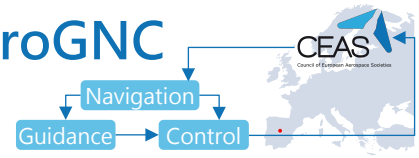

Madrid, Spain May 5th-7th 2026
uc3m Universidad Carlos III de Madrid
AIAA

GNSS-Flex: Evaluation of GNSS-SDR Receiver Prototypes Using High-Dynamic Target Drones

Iván Fernández Escribano Mechanical and Engineering (EM&E Group), Madrid, Spain.ifernandez@eme-es.es

Marc Majoral Centre Tecnològic de Telecomunicacions de Catalunya (CTTC/CERCA), Barcelona, Spain.marc.majoral@cttc.es

Xavier Guerrero Centre Tecnològic de Telecomunicacions de Catalunya (CTTC/CERCA), Barcelona, Spain.xavier.guerrero@cttc.es

Roberto Jiménez Escribano Mechanical and Engineering (EM&E Group), Madrid, Spain.rjimenez@eme-es.es

Mariano Madrid Escribano Mechanical and Engineering (EM&E Group), Madrid, Spain.mmadrid@eme-es.es

Javier Arribas Centre Tecnològic de Telecomunicacions de Catalunya (CTTC/CERCA), Barcelona, Spain.jarribas@cttc.es

Carles Fernández-Prades Centre Tecnològic de Telecomunicacions de Catalunya (CTTC/CERCA), Barcelona, Spain.cfernandez@cttc.es

Oscar Lozano Rosales Escribano Mechanical and Engineering (EM&E Group), Madrid, Spain.olozano@eme-es.es

Miguel Gómez-López Instituto Nacional de Técnica Aeroespacial (INTA), Madrid, Spain.gomezlma@inta.es

ABSTRACT

This paper presents results from the GNSS-Flex project, which evaluates software-defined GNSS receiver prototypes under demanding airborne conditions using SCRAB II target drones. These turbine-powered platforms, typically used as expendable targets, were adapted to host experimental receiver bays for testing advanced SDR architectures. Real flight data are analyzed, including receiver comparison, radar cross-check, and line-of-sight (LOS) dynamic assessment.

The SDR receivers achieved horizontal positioning accuracies within 10 m **(95th percentile) for SDR #1 and** 12 m **for SDR #2, with velocity errors below** 1 m s^{-1}**, maintaining robustness during aggressive maneuvers. Comparison with commercial reference units confirmed a high correlation of pseudorange, carrier-phase, and SNR observables. These results validate the feasibility of SDR-based GNSS architectures for resilient navigation in high-dynamic environments and show the suitability of target drones as testbeds. LOS-based PLL analysis reveals that the** 10 Hz **loop remains within stability limits, while the** 5 Hz **loop frequently exceeds them, leading to a predicted unlock rate of** 14.4 %**. These findings confirm that performance limitations under high dynamics are driven primarily by loop tuning rather than the SDR architecture itself.**

Keywords: GNSS, SDR receiver, high-dynamic flight test, resilient PNT, target drone

Nomenclature

B_n	=	Tracking-loop noise bandwidth
C/N_0	=	Carrier-to-noise density ratio
Δr	=	Position error
λ	=	GNSS carrier wavelength
ρ	=	Geometric range along the LOS
$\dot{\rho}$	=	LOS range rate
$\ddot{\rho}$	=	LOS range acceleration
j_{LOS}	=	LOS jerk (third time-derivative of range)
σ_t	=	Thermal tracking jitter (1-sigma)
σ_{eq}	=	Equivalent PLL margin, see Eq. (1)
θ_e	=	Deterministic dynamic-stress phase error
ω_0	=	Loop natural frequency
ζ	=	Loop damping ratio

1 Introduction

The design of resilient and flexible GNSS receivers remains a central challenge in aerospace and defence applications, where navigation systems must maintain robustness under high dynamics, severe Doppler evolution, harsh antenna attitudes, and potentially hostile signal conditions. Conventional hardware receivers, usually tuned for low- or medium-dynamic civil applications, can suffer degraded tracking or outright loss of lock when subjected to the accelerations and jerks typical of target drones, sounding rockets, and other aggressive flight profiles. In this context, software-defined radio (SDR) GNSS receivers are attractive because they provide full access to the acquisition and tracking chain, enable rapid parameter changes, and support direct experimentation with advanced loop strategies and interference-mitigation concepts [1–3].

The tracking problem under high dynamics is well established in the GNSS literature. Hinedi's early JPL analysis [4] already formalized the balance between loop bandwidth, thermal jitter, oscillator behaviour, and dynamic stress. These ideas were later consolidated in standard references such as Kaplan and Hegarty [3], where the classical lock conditions for DLLs, FLLs, and PLLs are expressed in terms of additive thermal and dynamic components. More recent work has extended these foundations toward hardware realizations and aided architectures, including optimized carrier-tracking loops [5, 6], oscillator-assisted tracking [7], and high-dynamic vector tracking or tightly coupled GNSS/INS approaches [8].

Experimental evidence at the high-dynamic end of the spectrum is still relatively scarce because it requires dedicated platforms, controlled instrumentation, and synchronized truth data. Representative flight campaigns have been carried out on sounding rockets and specialised research payloads [9–11], confirming that loop tuning is often the dominant factor once the signal-processing chain is otherwise sound.

GNSS-Flex addresses this gap with a repeatable airborne testbed based on SCRAB II target drones and in-house SDR receiver prototypes. The contribution of this paper is not only to present receiver-to-receiver comparisons, but also to connect those comparisons with a physics-based LOS dynamic-stress analysis derived from the exact RINEX observation epochs. That link is important because it helps distinguish architecture-level limitations from configuration-level limitations. In the present flight-2 dataset, the relative agreement between the SDRs and the commercial reference is good, whereas the most relevant weakness is clearly associated with an overly narrow PLL bandwidth in the advanced configuration.

2 Experimental Setup and Processing

The GNSS-Flex campaign was carried out using *SCRAB II* target drones, turbine-powered aerial platforms capable of sustained cruise speeds between approximately 75 m s^{-1} to 85 m s^{-1}. The aircraft were adapted to host an autonomous experimental bay for GNSS payloads, power conditioning, telemetry, and local data logging.

Two interchangeable payload bays were developed and validated before flight. A simplified view of both configurations is shown in Fig. 1.

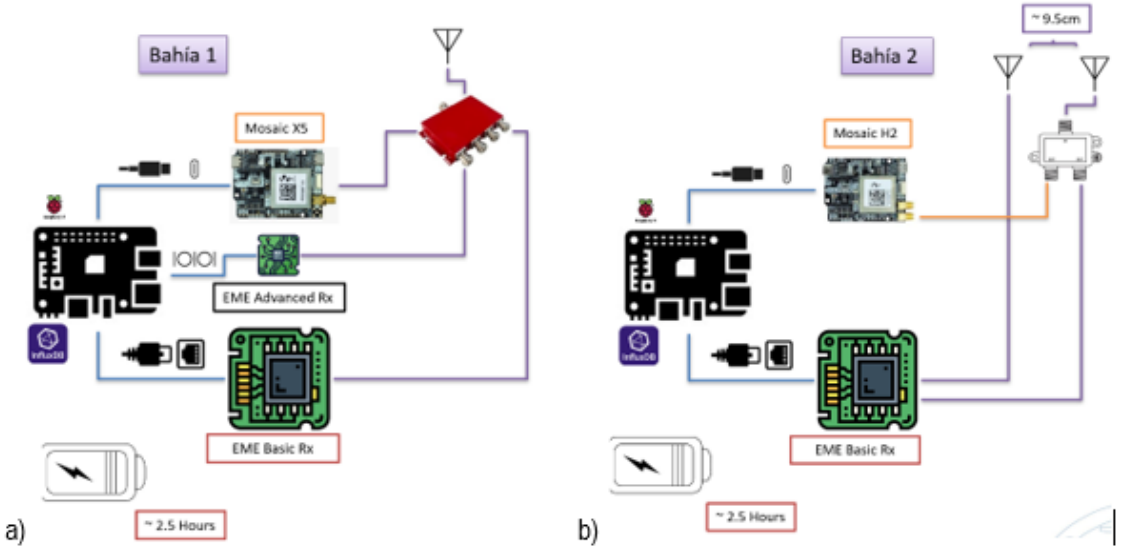

Fig. 1 Schematic representation of the experimental bays used in the campaign.

2.1 Bay Configurations

1) **Bay 1: single-antenna, multi-receiver payload.** This configuration used one broadband GNSS antenna feeding two SDR receivers and one Septentrio Mosaic-X5 through a common low-loss RF splitter. The arrangement was chosen to isolate digital processing effects by giving the three receivers the same antenna aperture and front-end conditions. A local clock board and a Raspberry Pi-based control subsystem handled power-up, timing, metadata, and autonomous logging.
2) **Bay 2: dual-antenna recording payload.** This configuration was intended for more advanced experiments, including spatial diversity and replay-based processing. It combined two antennas, one SDR chain, and an EM&E RF recording unit able to capture raw RF at up to 25 Msps with 2-byte quantization, enabling post-flight replay under modified tracking settings.

2.2 Flight Profiles and Ground Truth

The flights followed repeated *diabolo*-type trajectories at altitudes of roughly 500 m, combining climb, dive, and level segments that deliberately stress carrier tracking through changing LOS acceleration and jerk. The flight analysed in this paper extends over about 92 min of common GNSS observation time, from 08:06:18 UTC to 09:38:12 UTC, after synchronization between the observation RINEX and the reference trajectory.

Ground truth was provided by the INTA RIR-778 radar, an X-band system (8.5 GHz to 9.6 GHz) delivering time-stamped position data at 10 Hz with a range resolution of 3 m. In the current processing chain, radar data are used as an external absolute reference, while the Mosaic-X5 serves as the onboard reference receiver for relative SDR comparison.

Fig. 2 SCRAB II platform and INTA radar assets used during the campaign.

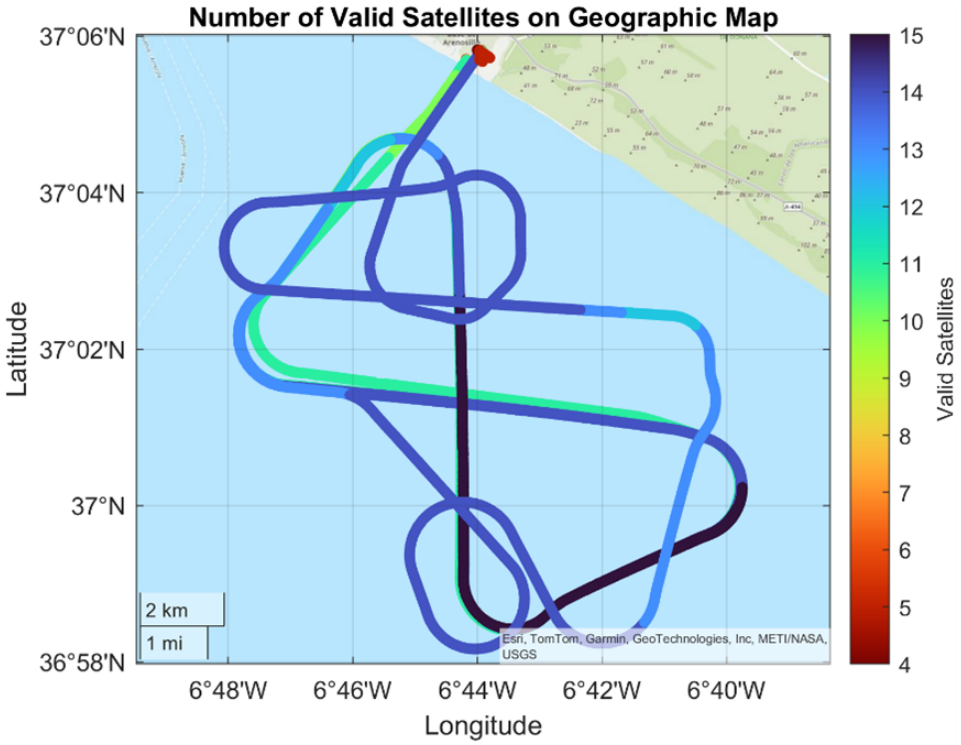

Fig. 3 Representative SCRAB II trajectory over the CEDEA range.

2.3 Receivers Under Test

The receiver configurations used in the analysis are summarized in Table 2. The basic SDR uses a conservative steady-state GPS PLL bandwidth of 10 Hz, whereas the advanced SDR narrows the GPS steady-state PLL to 5 Hz and has a separate frequency estimator during bandwidth transitions. For Galileo E1, the advanced receiver uses a third-order PLL at 20 Hz. These settings are directly reflected in the LOS dynamic-stress discussion in Section 3.3.

Table 2 Key tracking configurations used in the analysed flight. All bandwidths are steady-state (narrow-phase) values. The Mosaic-X5 Galileo DLL bandwidth is assumed equal to the GPS value; the internal Galileo configuration is not externally disclosed by Septentrio.

Receiver	GPS PLL/DLL [Hz]	Gal. PLL/DLL [Hz]	Notes
EME Rx basic	10 / 1	15 / 0.5	2nd-order GPS and Galileo
EME Rx advanced	5 / 2	20 / 2	GPS 2nd + high-dyn.; Galileo 3rd
Mosaic-X5	15 / 0.25	15 / 0.25[†]	Commercial reference

[†] Galileo DLL assumed equal to GPS; not disclosed by manufacturer.

2.4 Line Of Sight Analysis - dynamics stress

The observation RINEX epochs and the navigation RINEX were combined with the Septentrio trajectory to propagate each observed satellite at the exact observation times. Satellites below an elevation mask of 5° were excluded from the analysis. The PLL risk metric is defined as

$$\sigma_{eq} = \sigma_t + \frac{\theta_e}{3}, \tag{1}$$

which is algebraically equivalent to the standard criterion $3\sigma_t + \theta_e < 45°$ rearranged to a one-sigma form [3]. An epoch is classified as a predicted unlock event when $\sigma_{eq} > 15°$; the unlock fraction reported in Table 5 is the percentage of such epochs over the full common observation span.

For second-order PLLs, the deterministic dynamic-stress term was evaluated from the exact LOS radial acceleration,

$$\theta_e^{(2)} = \frac{360\,|\ddot{\rho}|}{\lambda\,\omega_0^2}, \qquad \omega_0 = \frac{2\pi B_n}{0.53}, \tag{2}$$

where the factor 0.53 follows from the second-order noise-bandwidth relation $B_n = \omega_0(4\zeta^2 + 1)/(8\zeta)$ evaluated at the optimal damping ratio $\zeta = 1/\sqrt{2}$ [3].

The third-order Galileo screening case used the jerk-driven form

$$\theta_e^{(3)} = \frac{360\,|j_{LOS}|}{\lambda\,\omega_0^3}, \qquad \omega_0 = \frac{2\pi B_n}{0.7845}, \tag{3}$$

where the factor 0.7845 is the standard third-order bandwidth coefficient from [3], Chapter 5, and j_{LOS} is the LOS jerk obtained as the central finite difference of $\ddot{\rho}$ at consecutive decimated epochs.

Importantly, $\ddot{\rho}$ was obtained from the full relative satellite–receiver kinematics rather than only from the receiver acceleration projection $-\mathbf{a}_{rx} \cdot \mathbf{u}_{LOS}$, preserving the actual geometry dependence satellite by satellite.

2.5 Tracking-Theory Reference

To interpret the flight-derived budgets, a companion closed-form theory model was kept strictly consistent with the Kaplan–Hegarty and Holmes bandwidth conventions [3, 4]. The same data-present criterion $\sigma_{eq} < 15°$ (Eq. 1) was applied with a pre-detection interval of 1 ms and a nominal operating point of 40 dB − Hz. This model is not intended as a deep threshold proof; its role here is to provide a compact, physically interpretable design reference.

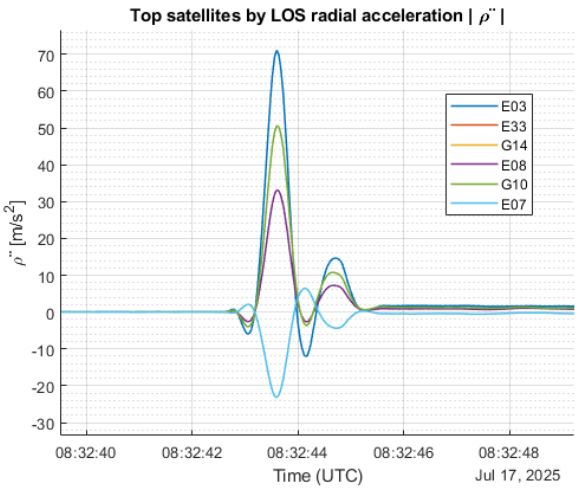

Fig. 4 LOS dynamics of the most affected satellites during launch

At this operating point, the thermal term alone remains small—1.31° to 2.63° across the tested configurations—so the dominant contribution in the stressed parts of the flight is the deterministic LOS term. Table 3 summarizes the resulting constant-stress limits. In particular, the 5 Hz second-order loop only tolerates about 0.20 g of LOS acceleration before crossing the 15° equivalent threshold, whereas the 10 Hz and 15 Hz loops extend that limit to 0.75 g and 1.64 g, respectively.

Table 3 Closed-form tracking reference limits at $C/N_0 = 40$ dB − Hz and $T = 1$ ms. For second-order loops the limit refers to constant LOS acceleration; for the third-order case it refers to constant LOS jerk.

Configuration	Ord.	B_n [Hz]	σ_t [deg]	Reference limit
EME Rx advanced (GPS)	2	5.0	1.31	$a_{LOS,\max} \approx 0.20\,g$
EME Rx basic (GPS)	2	10.0	1.86	$a_{LOS,\max} \approx 0.75\,g$
Mosaic-X5 (GPS)	2	15.0	2.27	$a_{LOS,\max} \approx 1.64\,g$
EME Rx advanced (Galileo E1)	3	20.0	2.63	$j_{LOS,\max} \approx 324.1\,\mathrm{m\,s^{-3}}$

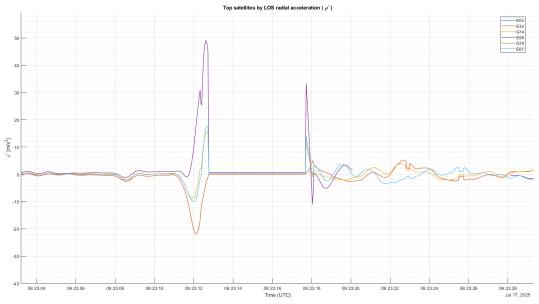

Fig. 5 LOS dynamics of the most affected satellites during parachute opening and ground touch down

3 Results

3.1 Relative Observables and PVT Consistency

At the relative-comparison level, the SDRs remain close to the Mosaic-X5 reference in both observables and navigation solution. Figures 6 and 7 show representative GPS and Galileo RINEX observables from the advanced receiver. Over most of the analysed interval, the tracked signals remain in the 35 dB − Hz to 45 dB − Hz region, with occasional fades and reacquisition events near the most dynamic parts of the trajectory.

The summary metrics extracted from the observable comparison files show mean C/N_0 values of 41.80 dB − Hz for the basic SDR, 41.78 dB − Hz for the advanced SDR, and 39.41 dB − Hz for the Mosaic-X5. Relative to the Mosaic-X5, the RMS C/N_0 mismatch is below 0.5 dB − Hz for both SDRs. The Doppler mismatch—which includes the effect of independent receiver clock-rate states and is therefore not directly comparable to sub-Hz carrier phase noise—is 99.5 Hz RMS for the advanced SDR and 233.4 Hz RMS for the basic SDR. The lower mismatch of the advanced receiver, despite its narrower steady-state PLL bandwidth, is attributed to its assisted mode, which maintains a dedicated frequency estimator during bandwidth transitions and therefore reports a more accurate instantaneous Doppler even when the steady-state PLL bandwidth is reduced.

The raw pseudorange differences are much larger, reaching 85.1 km RMS for the basic SDR and 91.4 km RMS for the advanced SDR. This result reflects the expected consequence of comparing unsynchronised receiver clock states in undifferenced pseudorange measurements and does not indicate a ranging-accuracy problem. The more informative quantities are the time evolution of the observables and the relative PVT consistency.

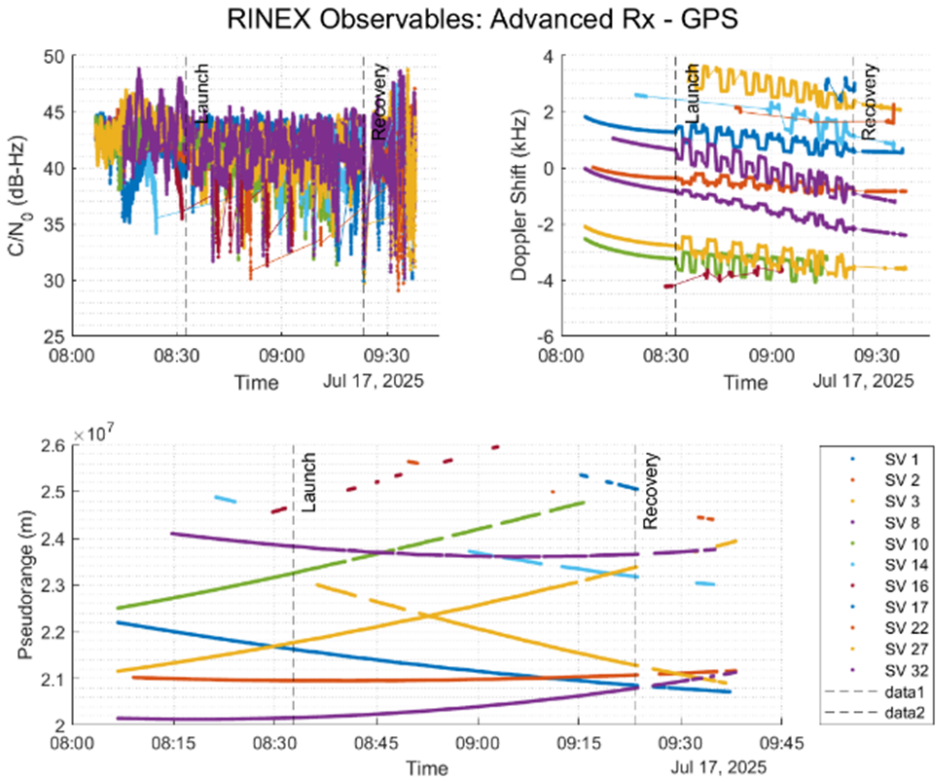

Fig. 6 Representative GPS observables from the advanced SDR receiver.

Figure 8 shows that the relative east/north position differences are centred close to zero. The mean east/north bias of the basic SDR with respect to the Mosaic-X5 is approximately $(-0.00,\ 0.10)$ m, while

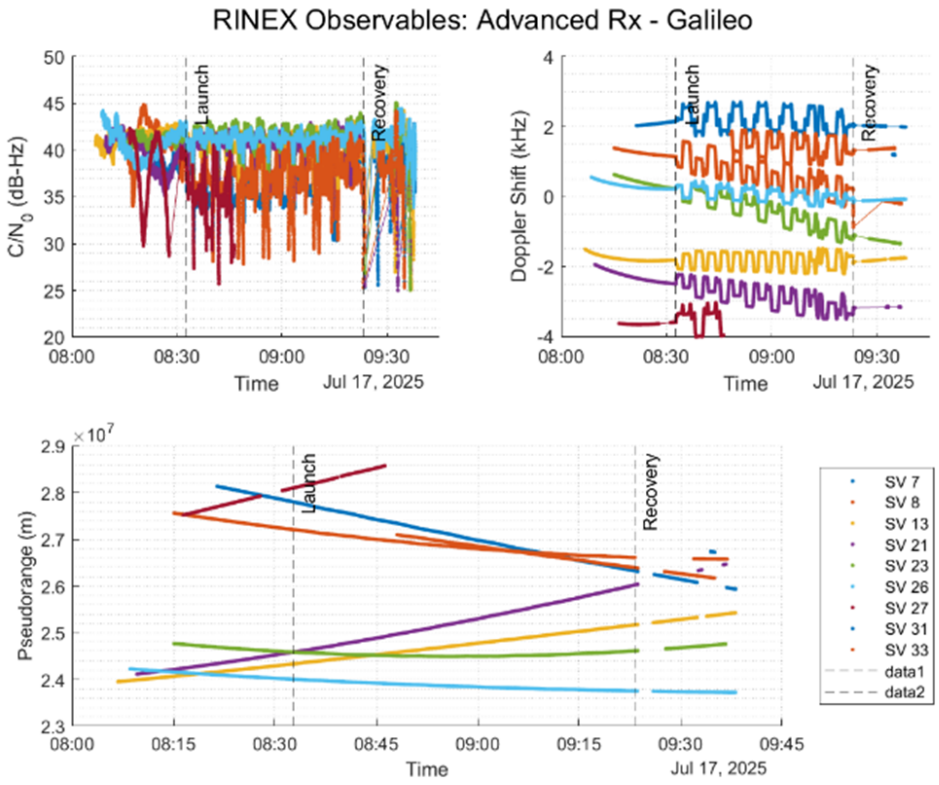

Fig. 7 Representative Galileo observables from the advanced SDR receiver.

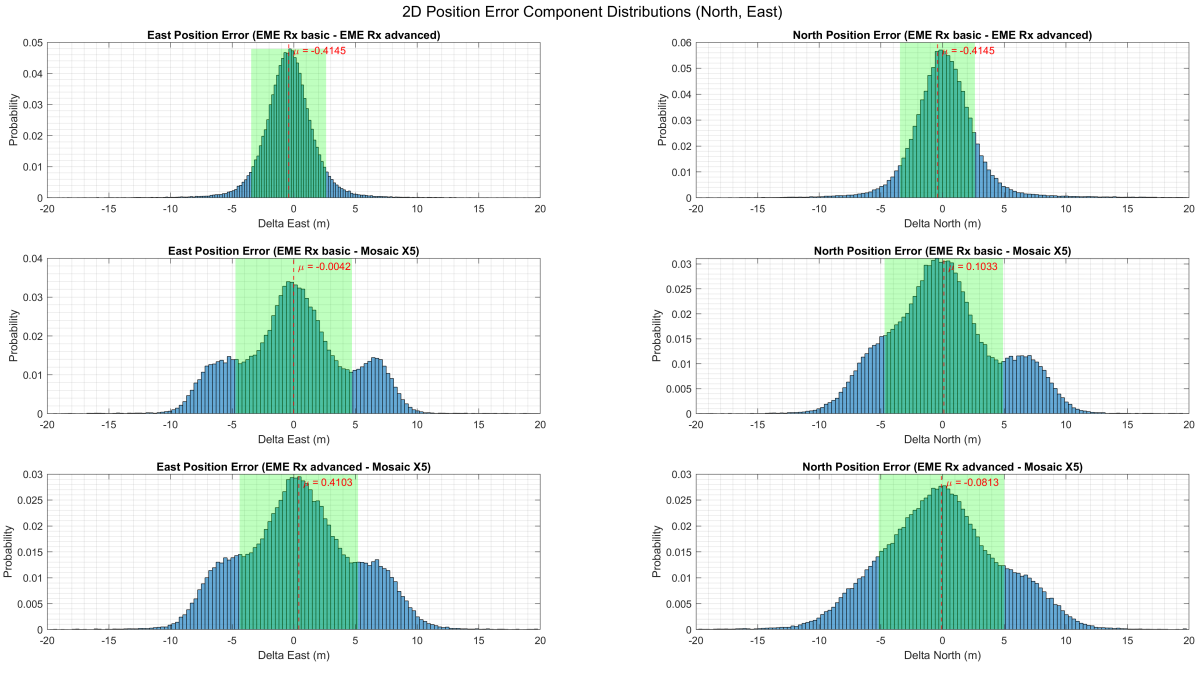

Fig. 8 Relative east/north position-difference distributions between the two SDRs and the Mosaic-X5 reference.

the advanced SDR exhibits (0.41, −0.08) m. Once the common trajectory is aligned in time, both SDRs remain close to the reference solution and the dominant differences appear in the spread of the distributions rather than in a large systematic horizontal offset.

3.2 Radar-Referenced Absolute Performance

Absolute performance was checked against the radar-derived trajectory. The horizontal error cumulative distribution for the in-flight phase is shown in Fig. 9. The current processing chain yields CEP95 values of approximately 13.0 m for both SDRs and 16.4 m for the Mosaic-X5, and CEP50 values of 3.9 m, 4.1 m, and 6.8 m, respectively.

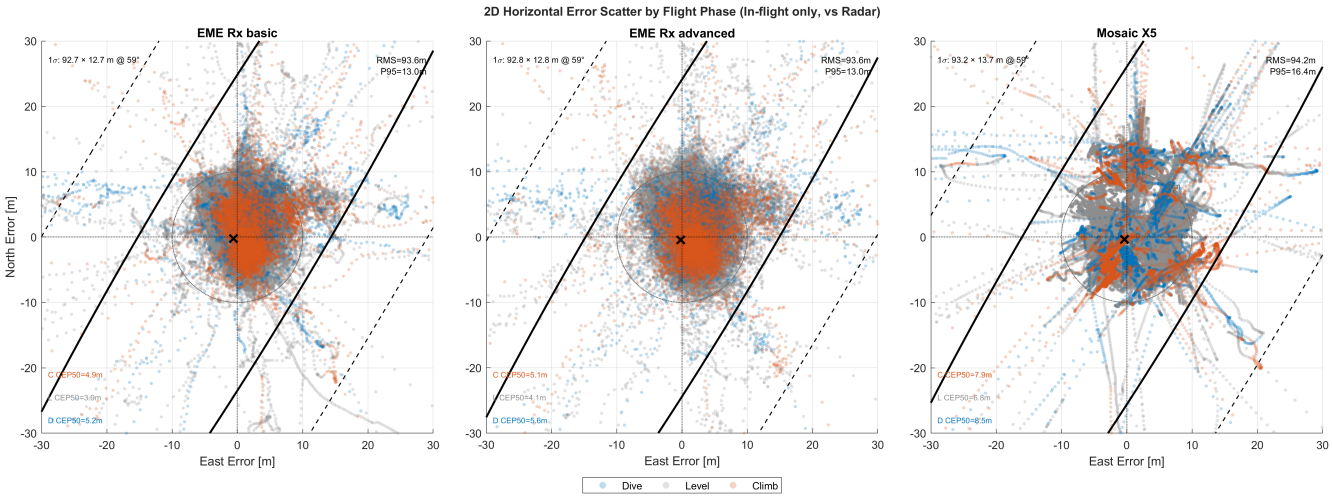

Fig. 9 2D horizontal position error scatter (East vs. North) relative to radar truth for all three receivers, restricted to the in-flight segment and colour-coded by flight phase (dive, level cruise, climb). Black solid and dashed ellipses indicate the 1σ and 2σ error covariance contours; the cross marks the mean bias. Climb-phase epochs (orange) produce the largest errors in the comercial receiver, consistent with the jerk-dominated onset of the pull-up manoeuvre.

Table 4 summarizes the current radar-based metrics. The absolute altitude error $|dZ|$ (95th percentile) refers to the absolute value of the signed height difference between each receiver and the radar truth, after geoid correction.

Table 4 Current radar-based metrics for the in-flight segment of the dataset. $|dZ|$ is the absolute value of the signed altitude error after geoid correction.

Metric	EME basic	EME advanced	Mosaic-X5
CEP50 [m]	3.9	4.1	6.8
CEP95 [m]	13.0	13.0	16.4
$\|dZ\|$ 95th percentile [m]	17.1	18.8	14.8
SEP95 [m]	20.8	22.6	20.3

The fact that the SDRs show lower CEP values than the Mosaic-X5 in the current radar-derived statistics warrants careful interpretation. Because the Mosaic-X5 is also used as the onboard reference for the relative SDR comparison, any systematic offset in its absolute trajectory would appear as a common bias in the relative distributions of Section 3.1, making the relative SDR metrics a lower bound on true absolute SDR accuracy rather than a direct absolute measure. If this ranking is confirmed after final radar re-alignment, that interpretation should be stated explicitly in the final version.

3.3 LOS Dynamic Stress and Tracking-Loop Margins

The most informative result for receiver design is the LOS dynamic-stress analysis because it uses the exact observation epochs and the actual satellite geometry. After trimming to the common reference span, the analysis used 13 290 epochs between 08:06:18 UTC and 09:38:12 UTC. Over most of the flight, between 6 and 8 GPS satellites and between 5 and 7 Galileo satellites above the 5° elevation mask were observed simultaneously. The high-dynamic portion of the reference trajectory starts shortly after 08:32 UTC, remains near 90 m s^{-1} for most of the airborne segment, and exhibits repeated acceleration bursts mostly in the 5 m s^{-2} to 10 m s^{-2} range with peaks close to 12 m s^{-2}. The worst PLL-budget excursions occur in this same interval.

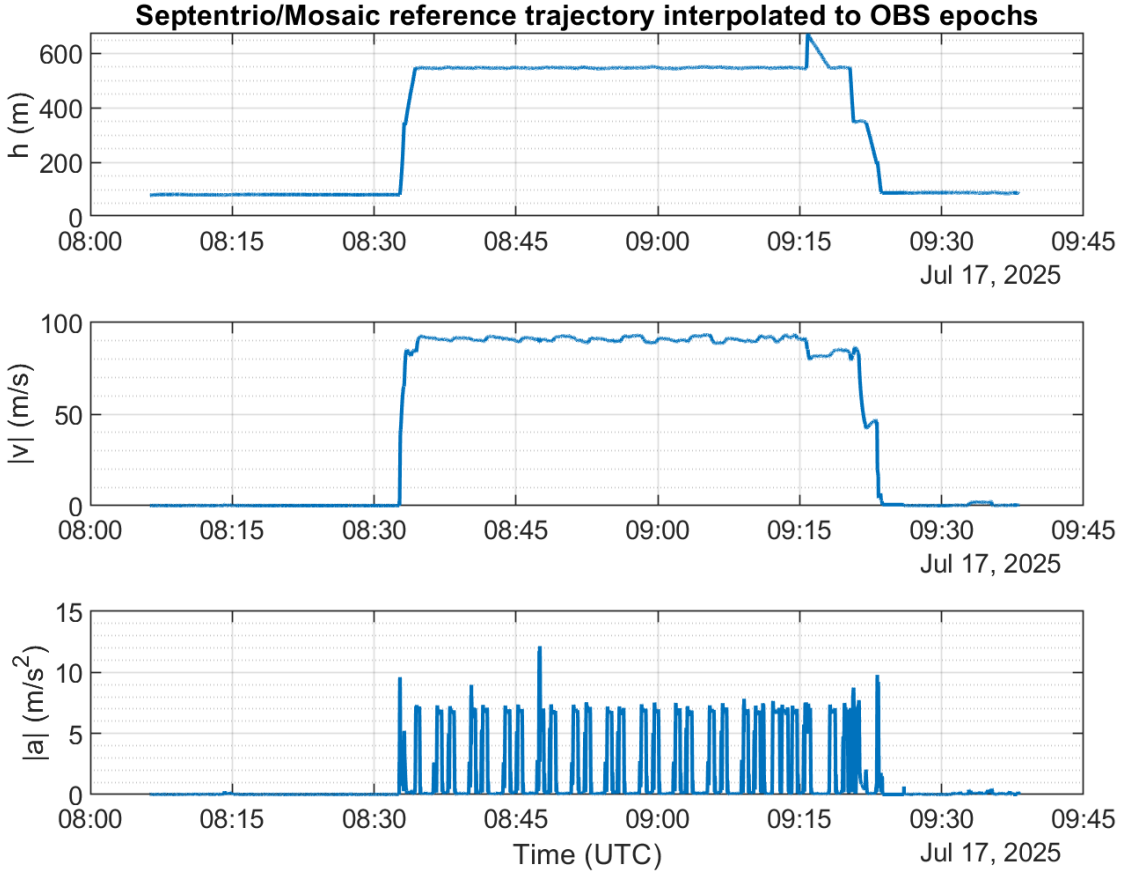

Fig. 10 Reference altitude, speed, and acceleration interpolated to the LOS-analysis epochs. The stressed tracking interval is concentrated in the airborne segment between approximately 08:32 UTC and 09:20 UTC.

The largest per-satellite LOS radial accelerations were associated with Galileo E03, whose P95 $|\ddot{\rho}|$ reached 8.9986 m s^{-2} and whose maximum reached 9.3469 m s^{-2}. The next most demanding satellites were G14, E33, E08, G10, and E07, all clustered around 5.8 m s^{-2} to 6.0 m s^{-2}. This confirms that the worst carrier-tracking stress is not uniform across the sky view but is concentrated in a relatively small subset of geometries.

Figure 12 and Table 5 show the central conclusion of the paper. The narrow 5 Hz advanced GPS PLL minimizes thermal noise but is too sensitive to dynamic stress for this flight profile. Its P95 worst-case σ_{eq} reaches 46.9°—well above the classical 15° design target—and the predicted unlock fraction rises to 14.4 %. It also reaches a maximum worst-case budget of 79.4°. By contrast, the basic 10 Hz PLL stays close to the limit with P95 14.2° and only occasional excursions to 26.9°, while the Mosaic-X5 15 Hz reference stays lower at P95 9.4° and maximum 19.9°. The EME Rx advanced Galileo third-order configuration at 20 Hz is the most robust in P95 terms, with only 0.11 % predicted unlock despite isolated short spikes up to 22.5°.

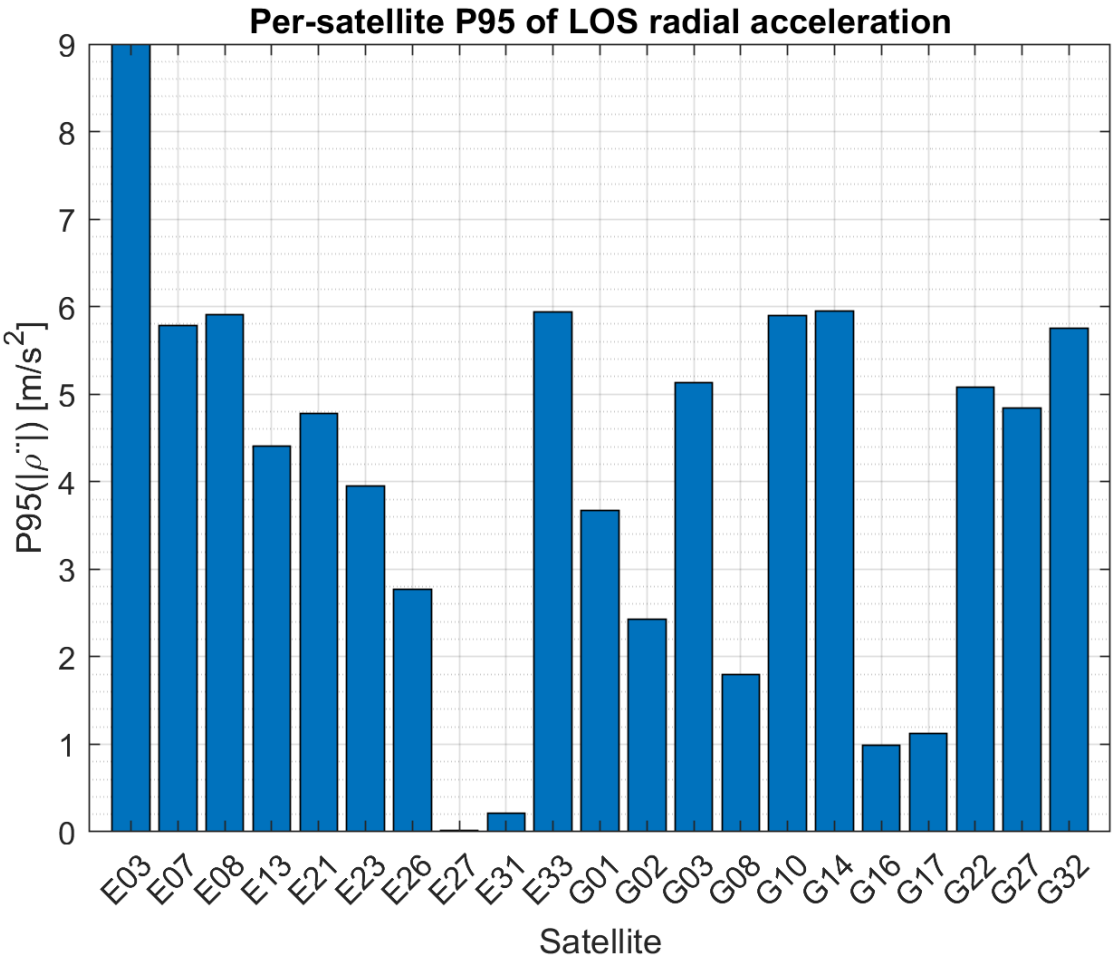

Fig. 11 Per-satellite P95 of LOS radial acceleration. The distribution is strongly geometry-dependent, with E03 clearly standing out from the rest of the observed set.

Table 5 PLL equivalent-budget summary from the LOS analysis (Eq. 1). Unlock fraction is the percentage of epochs for which $\sigma_{eq} > 15°$ over the full common observation span.

Configuration	Ord.	B_n [Hz]	P95 [deg]	Max [deg]	Unlock [%]
EME Rx basic (GPS)	2	10.0	14.18	26.90	0.29
EME Rx advanced (GPS)	2	5.0	46.91	79.43	14.42
Mosaic-X5 (GPS)	2	15.0	9.39	19.88	0.04
EME Rx advanced (Galileo E1)	3	20.0	7.90	22.51	0.11

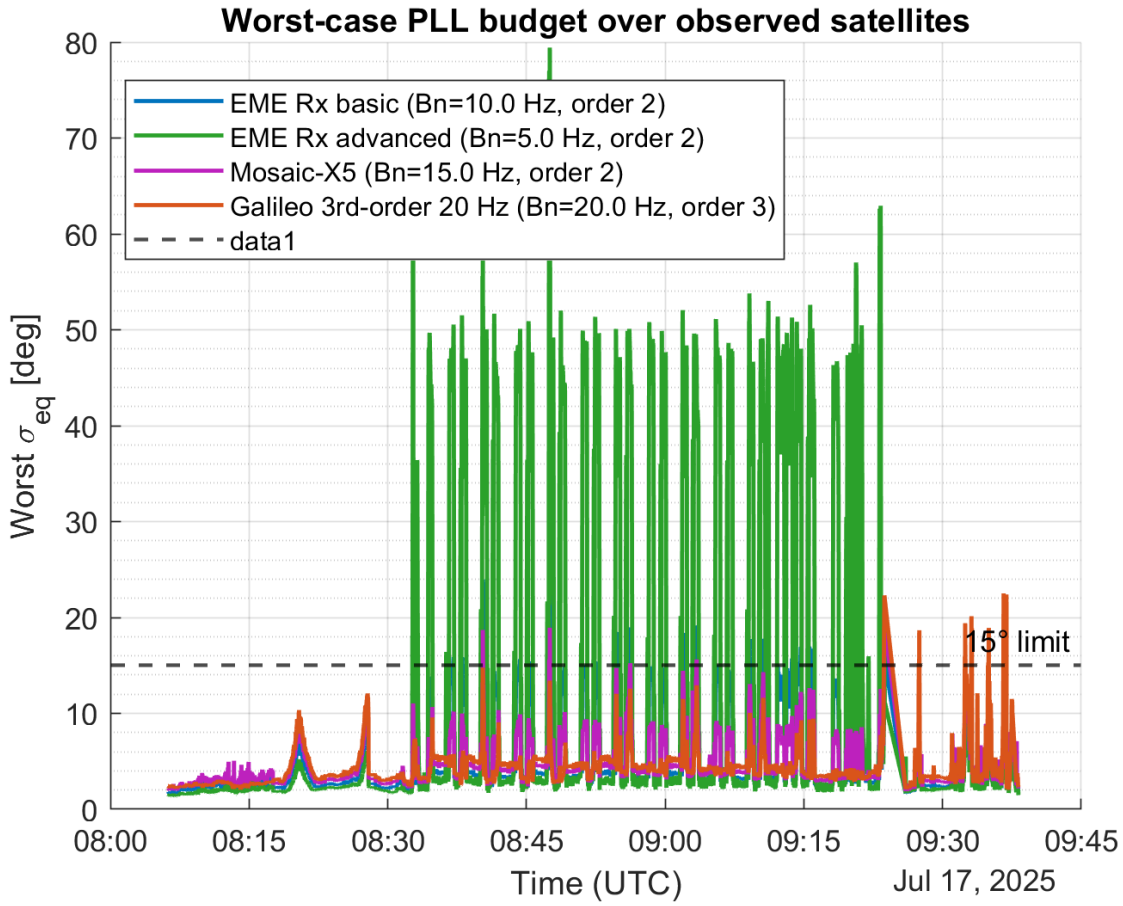

Fig. 12 Worst-case PLL equivalent budget σ_{eq} (Eq. 1) over all observed satellites as a function of time. The $15°$ lock limit is marked with a dashed line.

The agreement with the closed-form reference of Section 2.5 is not only qualitative. The E03 P95 stress of $8.9986\,\mathrm{m\,s^{-2}}$ corresponds to approximately $0.92\,g$ of LOS acceleration. At the nominal $40\,\mathrm{dB-Hz}$ operating point, this exceeds the theoretical 5 Hz tolerance by more than a factor of four, slightly exceeds the 10 Hz tolerance, and is comfortably below the 15 Hz tolerance. Evaluated with Eq. (2), that single-satellite P95 stress yields approximate σ_{eq} values of 65.1°, 17.8°, and 9.4° for the 5 Hz, 10 Hz, and 15 Hz second-order loops, respectively—the same ranking observed in the flight-derived Table 5.

This comparison also clarifies that the problem is dynamics-dominated rather than thermal-noise-dominated. At $40\,\mathrm{dB-Hz}$, the thermal term alone is only 1.3° to 2.3° for the second-order loops considered here, whereas the dynamic term drives the 5 Hz configuration far beyond the lock limit during the stressed interval. For the EME Rx advanced Galileo 20 Hz third-order case, the E03 P95 jerk of $4.1542\,\mathrm{m\,s^{-3}}$ is far below the constant-jerk reference limit of $324.1\,\mathrm{m\,s^{-3}}$, consistent with its low P95 worst-case budget of 7.9°. The results therefore support a clear engineering conclusion: in this trajectory, the advanced receiver is not limited by its open SDR architecture, but by a steady-state GPS PLL that is too narrow for the realised LOS acceleration profile.

4 Discussion

Three main observations can be drawn from the current state of the dataset.

To begin with, the open SDR receivers consistently reproduce the behaviour of the reference receiver at a relative level. The agreement observed in the signal traces, together with the low C/N_0 mismatch and the small mean east/north PVT biases, indicates that the signal-processing chain is operating reliably. This provides important validation of the front-end, correlator, and navigation data flow.

In addition, the comparison with radar measurements is informative, although it is not yet fully consolidated. The Mosaic-X5 serves as the onboard relative reference, yet it appears to be outperformed by the SDRs in terms of absolute CEP. Should this ranking be confirmed after the final radar re-alignment, the relative SDR metrics presented in Section 3.1 would need to be interpreted as conservative lower bounds on their true absolute accuracy. This follows from the fact that any systematic offset in the Mosaic-X5 would manifest as a common bias in the relative distributions. At present, however, the velocity comparison against radar still exhibits clear anomalies and requires further refinement.

Finally, the line-of-sight (LOS) analysis provides key insight into why the advanced receiver does not surpass the basic configuration during the most dynamic intervals. The more conservative basic setup remains close to the classical PLL stability limit, whereas the advanced configuration, with its 5 Hz loop bandwidth, frequently exceeds this threshold. The comparison with closed-form theoretical predictions is particularly revealing: the measured LOS stresses align with the same side of the predicted 5 Hz, 10 Hz, and 15 Hz limits as indicated by the flight-based performance ranking. Moreover, the analysis highlights that the dominant stress driver is the instantaneous LOS acceleration, which varies across satellites and is concentrated in specific geometries, rather than a single platform-level acceleration metric.

5 Conclusions

This paper has presented the results for two in-house SDR receivers and one Mosaic-X5 reference receiver flown on a SCRAB II target drone. The relative receiver comparison shows that the SDRs follow the reference observables closely and maintain sub-metre mean horizontal biases with respect to the Mosaic-X5 trajectory. The radar-referenced absolute comparison places the three receivers in the same overall performance class—horizontal errors in the 10 m to 20 m range—although the final velocity-based validation still requires one further processing iteration.

The clearest technical result is provided by the LOS dynamic-stress analysis. For the analysed trajectory, a 10 Hz second-order PLL is close to the classical design threshold but remains largely viable, whereas a 5 Hz second-order PLL becomes too sensitive to LOS acceleration and produces a much higher predicted unlock probability. The flight-derived ranking agrees with the book-consistent theory reference (Eqs. 2 and 3) and shows that dynamic stress, not thermal jitter, is the dominant carrier-tracking limitation in this dataset. The paper therefore supports the practical conclusion that open SDR GNSS receivers are viable for this class of airborne platform, provided the tracking-loop configuration is matched to the actual flight dynamics and to the realised per-satellite LOS geometry.

Future Work

The next step is to use the available raw IQ recordings to replay the high-dynamic segments with alternative loop bandwidths and adaptive bandwidth schedules. The present LOS analysis already indicates that bandwidth adaptation keyed to estimated LOS acceleration will be more valuable than simply narrowing the PLL for thermal-noise reasons alone. Those replay campaigns should be used to check how closely actual loss-of-lock events follow the LOS-derived σ_{eq} predictor and to determine whether phase-dependent or adaptive bandwidth control can keep the carrier loop inside the theoretical margin without sacrificing quiet-flight precision.

Acknowledgments

This work has been partially supported by the Spanish Ministry of Science and Innovation under grant CPP2021-008648, funded by AEI/10.13039/501100011033 and co-financed by the European Union (NextGenerationEU/PRTR).

Declaration of Use of Artificial Intelligence

Artificial intelligence tools were employed solely to check grammar, enhance readability, and improve the clarity of the text in previously written sections. These tools were not used to generate scientific content, formulate answers to the presented research problems, or interpret experimental results. The authors have carefully reviewed and edited all AI-assisted text as needed and take full responsibility for the content of this publication.

References

[1] C. Fernández–Prades, J. Arribas, and P. Closas. Robust GNSS receivers by array signal processing: Theory and implementation. *Proceedings of the IEEE*, 104(6):1207–1220, June 2016. doi: 10.1109/JPROC.2016.2532963.

[2] J. Arribas, C. Fernández-Prades, and P. Closas. GNSS-SDR: An open source tool for researchers and developers. In *Proc. ION GNSS+*, pages 780–794, 2013.

[3] E. Kaplan and C. Hegarty. *Understanding GPS/GNSS: Principles and Applications*. Artech House, 3rd edition, 2017.

[4] S. Hinedi. High-dynamic GPS tracking. *Jet Propulsion Laboratory (JPL) Technical Report*, JPL Report 1988-10742, 1988.

[5] Pedro A. Roncagliolo, Javier G. García, and Carlos H. Muravchik. Optimized carrier tracking loop design for real-time high-dynamics gnss receivers. *International Journal of Navigation and Observation*, 2012:1–18, 2012. doi: 10.1155/2012/651039.

[6] Pedro A. Roncagliolo and Javier G. García. A new tracking loop scheme for high dynamics real-time gnss receivers with hardware correlators. In *Proc. of the 29th International Technical Meeting of the Satellite Division of The Institute of Navigation (ION GNSS+ 2016)*, pages 427–435, 2016. doi: 10.33012/2016.14836.

[7] Maryam Abedi, Tian Jin, and Kewen Sun. Gnss signal tracking performance improvement for highly dynamic receivers by gyroscopic mounting crystal oscillator. *Sensors*, 15(10):21673–21695, 2015. doi: 10.3390/s150921673.

[8] R. Mu, Y. Dong, and G. Zhao. Design and implementation of vector tracking loop for high-dynamic gnss receiver. *Sensors*, 21(16):5629, 2021. doi: 10.3390/s21165629.

[9] Iñigo Cortés Vidal, Santiago Urquijo, Matthias Overbeck, Wolfgang Felber, Loukis Agrotis, Volker Mayer, Erik Schönemann, and Werner Enderle. Robust tracking strategy for modern gnss receivers in sounding rockets. In *2022 10th Workshop on Satellite Navigation Technology (NAVITEC)*, 2022. doi: 10.1109/NAVITEC53682.2022.9847547.

[10] Moritz Aicher, Benjamin Braun, and Markus Markgraf. Kodiak: A versatile special purpose multi-gnss receiver for highly dynamic sounding rocket applications. In *European Space Agency (ESA) Conference, 2022*, 2022. See DLR document 'KODIAK: . . . '. `https://elib.dlr.de/187866/1/A-082aicher.pdf`.

[11] A. Grillenberger et al. Flight test results of a novel integrated gps receiver for high dynamics. In *ESA Space Propulsion Conference & Exhibition, 2011 (or ESA SP-700?)*, page —, 2011. "Flight Test Results of a Novel Integrated GPS Receiver for . . . ".